Available online at www.sciencedirect.com
ScienceDirect
Journal of Solid State Chemistry 180 (2007) 1902–1910
JOURNAL OF SOLID STATE CHEMISTRY
www.elsevier.com/locate/jssc

Oxygen non-stoichiometry of $Ln_4Ni_{2.7}Fe_{0.3}O_{10-\delta}$ (Ln = La, Pr)

E.V. Tsipis[a,b], M.V. Patrakeev[c], J.C. Waerenborgh[b], Y.V. Pivak[a], A.A. Markov[c], P. Gaczyński[b], E.N. Naumovich[a,d], V.V. Kharton[a,d,*]

[a]Department of Ceramics and Glass Engineering, CICECO, University of Aveiro, 3810-193 Aveiro, Portugal
[b]Chemistry Department, ITN/CFMC-UL, Estrada Nacional 10, P-2686-953 Sacavém, Portugal
[c]Institute of Solid State Chemistry, UB RAS, 91 Pervomaiskaya Str., 620219 Ekaterinburg, Russia
[d]Institute of Physicochemical Problems, Belarus State University, 14 Leningradskaya Str., 220050 Minsk, Belarus

Received 9 February 2007; received in revised form 13 April 2007; accepted 13 April 2007
Available online 8 May 2007

Abstract

The oxygen deficiency of iron-substituted nickelates $Ln_4Ni_{2.7}Fe_{0.3}O_{10-\delta}$ (Ln = La, Pr) with the orthorhombic Ruddlesden-Popper structure was studied by thermogravimetric analysis and coulometric titration in the oxygen partial pressure range 6×10^{-5} to 0.7 atm at 973–1223 K. In air, the non-stoichiometry values vary in the relatively narrow ranges $(2.4-4.2)\times10^{-2}$ for La- and $(0.01-2.0)\times10^{-2}$ for Pr-containing compositions, increasing with temperature. Due to the smaller size of praseodymium cations, $Pr_4Ni_{2.7}Fe_{0.3}O_{10-\delta}$ exhibits a substantially lower thermodynamic stability in comparison with $La_4Ni_{2.7}Fe_{0.3}O_{10-\delta}$ and $La_4Ni_3O_{10-\delta}$, although the oxygen content in $Pr_4Ni_{2.7}Fe_{0.3}O_{10-\delta}$ lattice is higher. The partial substitution of iron for nickel has no essential effect on the low-$p(O_2)$ stability limit corresponding to the transition of $Pr_4Ni_3O_{10-\delta}$ into K_2NiF_4-type $Pr_2NiO_{4+\delta}$. On the contrary, doping of $La_4Ni_3O_{10-\delta}$ with iron decreases the oxygen vacancy concentration and shifts the phase stability boundary towards lower oxygen chemical potentials, suggesting a stabilization of the transition metal-oxygen octahedra in lanthanum nickelate lattice. The Mössbauer spectroscopy showed that the predominant state of iron cations, statistically distributed between the nickel sites, is trivalent.

Keywords: Ruddlesden-Popper nickelates; Oxygen deficiency; Mössbauer spectroscopy; Thermogravimetry; Coulometric titration; Oxygen thermodynamics; Phase stability

1. Introduction

Mixed conductors derived from K_2NiF_4-type lanthanum nickelate, $La_2NiO_{4+\delta}$, are of great interest for high-temperature electrochemical applications, such as the cathodes of solid oxide fuel cells (SOFCs) and the dense ceramic membranes for oxygen separation and partial oxidation of light hydrocarbons [1–8]. Important advantages of La_2NiO_4-based materials include relatively high oxygen-ionic and p-type electronic conductivities, moderate thermal and chemical expansion, and high electrocatalytic activity under oxidizing conditions. $La_2NiO_{4+\delta}$ is the first member of the Ruddlesden-Popper series (LaO)$(LaNiO_3)_n$, with $n=1$. The intergrowth structure of this compound consists of perovskite-like NiO_2 layers alternating with rock-salt La_2O_2 sheets, which may accommodate a significant oxygen excess; the incorporation of mobile O^{2-} interstitials is charge-compensated by the formation of electron holes localized on nickel cations [2–4,6,9,10]. The concentration of oxygen vacancies in the perovskite layers of undoped $La_2NiO_{4+\delta}$ is very low [9,10]. The lattice symmetry can vary from tetragonal (space groups $I4/mmm$ or $F4/mmm$) to orthorhombic (space groups $Fmmm$ and $Cmca$), depending on oxygen chemical potential and temperature [10,11]. Compared to other phases existing in the ternary La–Ni–O system, $La_2NiO_{4+\delta}$ has maximum stability on reducing oxygen partial pressure and on increasing temperature [12,13]. Doping with higher-valence cations, such as iron, rises the concentration of interstitial

*Corresponding author. Department of Ceramics and Glass Engineering, CICECO, University of Aveiro, 3810-193 Aveiro, Portugal.
Fax: +351 234 425300.
E-mail address: kharton@cv.ua.pt (V.V. Kharton).

0022-4596/$ - see front matter © 2007 Elsevier Inc. All rights reserved.
doi:10.1016/j.jssc.2007.04.025

anions, whereas thermodynamic stability of substituted $La_2NiO_{4+\delta}$ in reducing atmospheres remains essentially unchanged [7,14].

Increasing the number of perovskite layers in the Ruddlesden-Popper (RP) nickelates, n, leads to faster ionic and electronic transport [2,3,11,15]. These effects are primarily associated with increasing concentration of Ni−O−Ni bonds responsible for the electronic conduction, progressive delocalization of the p-type electronic charge carriers, and increasing vacancy-migration contribution to oxygen ion diffusivity. Note that, except for $La_2NiO_{4+\delta}$, all RP nickelates are oxygen-deficient at elevated temperatures [11,13]. As a particular consequence, the electrochemical activity of $La_{n+1}Ni_nO_{3n+1-\delta}$ cathodes becomes substantially higher when n increases from 1 to 3 [2]; analogous results were also obtained for the praseodymium nickelate electrodes where $Pr_4Ni_3O_{10-\delta}$ phase is formed due to oxidative decomposition of $Pr_2NiO_{4+\delta}$ [16]. The maximum electrode performance might hence be expected for perovskite-type $LnNiO_{3-\delta}$ (Ln = La, Pr). However, these perovskites are unstable at temperatures above 1200–1300 K in oxidizing conditions [12,13,15] and may decompose under cathodic polarization. The thermodynamic stability of $La_4Ni_3O_{10-\delta}$ is higher than that of $LaNiO_{3-\delta}$ and $La_3Ni_2O_{7-\delta}$ [13]. Also, as $La_4Ni_3O_{10-\delta}$ lattice (Fig. 1) may contain a significant amount of oxygen vacancies in the perovskite layers connected along the b-axis [13], further improvement can be achieved by the partial substitution of nickel with donor-type cations in order to stabilize the transition metal–oxygen octahedra. The information on redox behavior of RP nickelates and, in particular, on the Ni-site doping effects is however scarce. Continuing our research on nickelate-based mixed conductors [6–9,14,16], the present work is focused on the analysis of oxygen non-stoichiometry and iron oxidation states in $Ln_4Ni_{2.7}Fe_{0.3}O_{10-\delta}$ (Ln = La, Pr).

2. Experimental

Submicron powders of $La_4Ni_{2.7}Fe_{0.3}O_{10-\delta}$ and $Pr_4Ni_{2.7}Fe_{0.3}O_{10-\delta}$ were prepared by the glycine-nitrate process [17]. The synthesized powders were annealed in air at 1273–1373 K for 20–22 h with several intermediate regrinding steps, and then slowly cooled (1–2 K/min) in order to achieve equilibrium with atmospheric oxygen at low temperatures. Additional series of samples used for the analysis of phase composition at elevated temperatures, were also annealed in various atmospheres and then quenched in liquid nitrogen. The crystal structure was studied by X-ray diffraction (XRD) using a Rigaku D/Max-B instrument (CuK_α radiation, $2\theta = 10$–100°, step 0.02°, 8–10 s/step) and selected-area electron diffraction (SAED) using a Hitachi H-9000 transmission electron microscope. The total oxygen content at atmospheric oxygen partial pressure was determined by thermogravimetric analysis (TGA, Setaram SetSys 16/18, weight resolution of 0.4 μg; sample weight of 650–800 mg). The TGA procedures included both heating with a constant rate (2 K/min) in flowing dry air, and temperature cycling in the range 973–1323 K with 50 K steps and equilibration at each temperature during 1–3 h. The equilibration criterion was selected as the weight relaxation rate ($\Delta m/\Delta\tau$) lower than 15 μg/h, with the second derivative $\partial^2 m/m_0\partial\tau^2\partial$ higher than -2×10^{-4}%/h. After the measurements in air, the apparatus was flushed with argon at 1323 K and the samples were reduced in a flow of dry 10% H_2–90% N_2 mixture for 10 h, with subsequent heating up to 1423 K in the same flow in order to ensure complete reduction of nickel and iron. The isothermal reduction procedure is illustrated by Fig. 2. The oxygen stoichiometry variations on changing oxygen partial pressure, $p(O_2)$, were studied at 1023–1223 K by coulometric titration (CT)

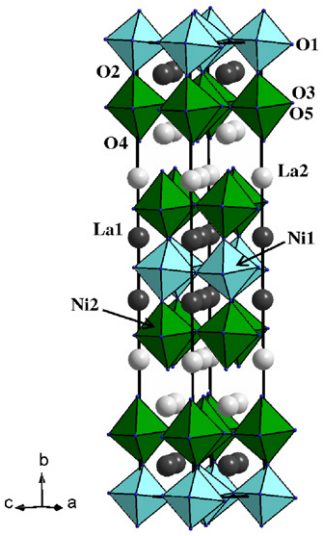

Fig. 1. Crystal structure of orthorhombic $La_4Ni_{2.7}Fe_{0.3}O_{10}$ (space group *Cmca*).

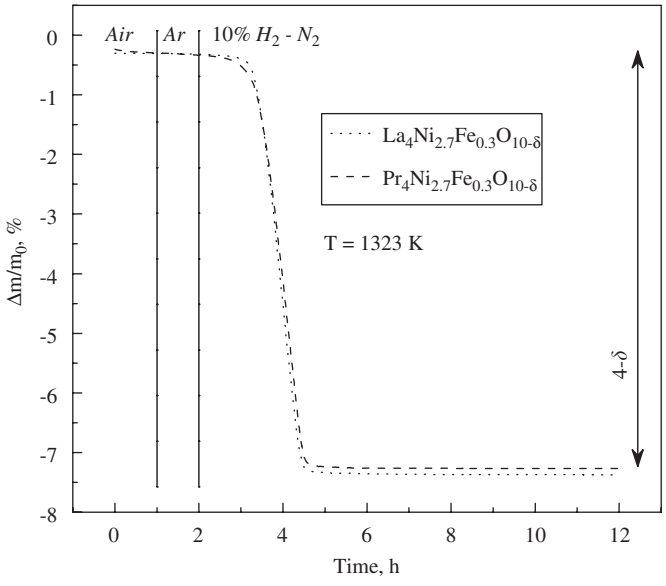

Fig. 2. Determination of the total oxygen content in $La_4Ni_{2.7}Fe_{0.3}O_{10-\delta}$ and $Pr_4Ni_{2.7}Fe_{0.3}O_{10-\delta}$ powders at 1323 K by the TGA technique.

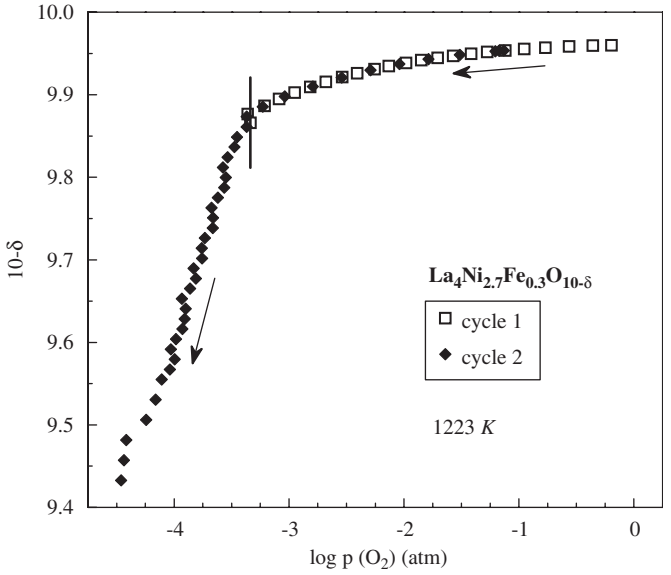

Fig. 3. Example of the coulometric titration data, showing reproducibility of the oxygen content variations in $La_4Ni_{2.7}Fe_{0.3}O_{10-\delta}$ on cycling oxygen pressure at 1223 K. Arrows indicate the direction of $p(O_2)$ changes. The solid line shows approximate low-$p(O_2)$ phase boundary.

technique, as described elsewhere [18]. The CT experiments were performed in an isothermal regime, varying $p(O_2)$ from 6×10^{-5} to 0.7 atm; then the titration cycles at 1023 and 1223 K were repeated in a wider range of the oxygen partial pressure, down to 10^{-10} atm. The results obtained on cycling $p(O_2)$ showed an excellent reproducibility, as illustrated in Fig. 3 by the example of $La_4Ni_{2.7}Fe_{0.3}O_{10-\delta}$; this confirmed zero leakage in the CT cells.

The Mössbauer spectroscopy data were collected in transmission mode using a conventional constant-acceleration spectrometer and a 25 mCi ^{57}Co source in a Rh matrix. Considering the relatively low iron content and high-electronic mass-absorption coefficient for the 14.4 keV radiation, $La_4Ni_{2.7}Fe_{0.3}O_{10-\delta}$ powder for the Mössbauer spectroscopy studies was synthesized using metallic iron enriched with ^{57}Fe isotope (49% ^{57}Fe, Chemgas, France); the preparation conditions were identical to those used for the samples with natural iron. The absorbers containing 0.25 mg/cm^2 of iron enriched with ^{57}Fe were obtained by pressing into a perspex holder. The $Pr_4Ni_{2.7}Fe_{0.3}O_{10-\delta}$ absorber was prepared from the powder containing natural Fe; due to very low ^{57}Fe content, the absorber thickness was calculated on the basis of the electronic mass-absorption coefficient according to Ref. [19]. The velocity scale was calibrated using α-Fe foil. The low-temperature Mössbauer spectra were collected using a JANIS bath cryostat (model SVT-400). The isomer shifts (IS, Table 1) are given relative to metallic α-Fe at 295 K. The spectra were fitted to Lorentzian lines using a non-linear least-squares method [20]. In the course of refinement procedure, the relative areas and line widths of each peak in a quadrupole doublet and peaks 1–6, 2–5 and 3–4 in a magnetic sextet were constrained to remain equal.

Table 1
Parameters estimated from the Mössbauer spectra of $Ln_4Ni_{2.7}Fe_{0.3}O_{10+\delta}$ equilibrated in air at low temperatures, taken at 295 and 4 K

Composition	T (K)	IS (mm/s)	QS, ε (mm/s)	B_{hf} (T)	Γ (mm/s)	I (%)
$La_4Ni_{2.7}Fe_{0.3}O_{10+\delta}$	295	0.30	0.72	–	0.39	68
		0.28	0.26	–	0.22	32
	4	0.42	−0.04	42.0	0.62	69
		0.42	−0.26	46.7	0.70	31
$Pr_4Ni_{2.7}Fe_{0.3}O_{10+\delta}$	295	0.28	0.64	–	0.44	100

IS, QS, ε, B_{hf}, Γ and I are the isomer shift relative to metallic α-Fe at 295 K, quadrupole splitting or quadrupole shift, magnetic hyperfine field, full width at half maximum, and relative area, respectively. Estimated standard deviations are <3% for I, <0.2 T for B_{hf} and <0.02 mm/s for the other parameters.

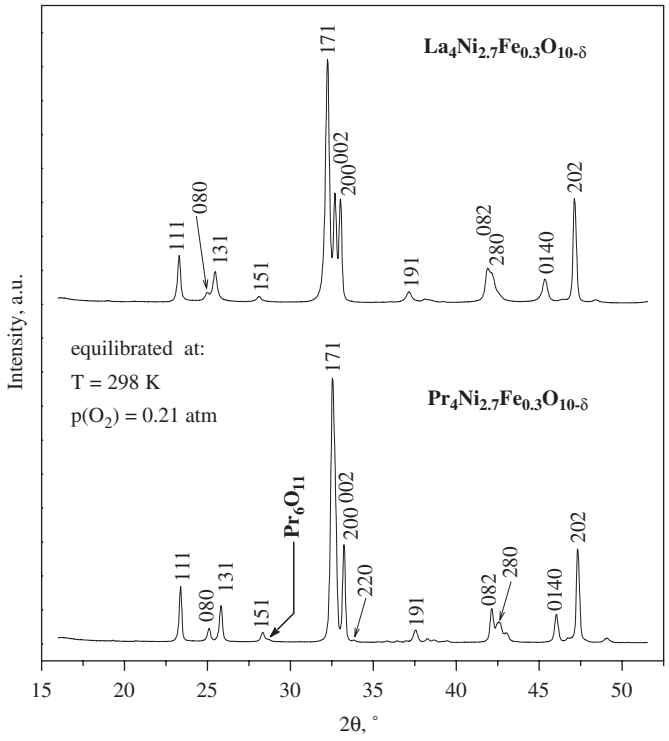

Fig. 4. XRD patterns of $La_4Ni_{2.7}Fe_{0.3}O_{10+\delta}$ and $Pr_4Ni_{2.7}Fe_{0.3}O_{10+\delta}$, equilibrated with atmospheric oxygen at low temperatures. For the major reflections, the *hkl* indices are shown.

3. Results and discussion

The XRD and SAED analyses of as-synthesized $Ln_4Ni_{2.7}Fe_{0.3}O_{10}$ confirmed formation of orthorhombic RP phases; the space group was identified as *Cmca*, in agreement with literature [21]. No extra reflections were detected in the XRD pattern of $La_4Ni_{2.7}Fe_{0.3}O_{10}$ (Fig. 4). In the case of $Pr_4Ni_{2.7}Fe_{0.3}O_{10}$, very minor peaks corresponding to Pr_6O_{11} were observed. The separation of a small amount of praseodymium oxide, known also for parent $Pr_4Ni_3O_{10}$ [11], may be associated with surface oxidation of Pr cations, which are predominantly trivalent

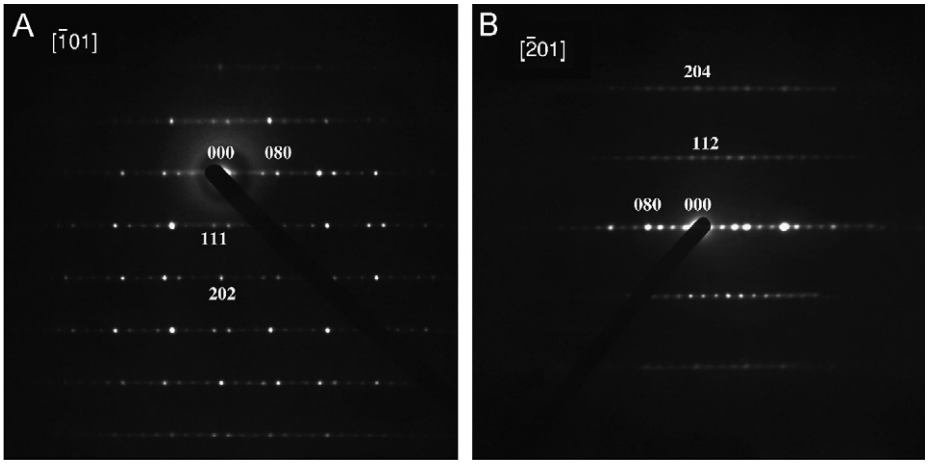

Fig. 5. Selected area electron diffraction patterns of $La_4Ni_{2.7}Fe_{0.3}O_{10+\delta}$ (A) and $Pr_4Ni_{2.7}Fe_{0.3}O_{10+\delta}$ (B).

Table 2
Unit cell parameters and oxygen hyperstoichiometry of $Ln_4Ni_{2.7}Fe_{0.3}O_{10+\delta}$ (space group *Cmca*) equilibrated with atmospheric oxygen at low temperatures

Ln	Lattice parameters (Å)			Unit cell volume (Å^3)	δ
	a	*b*	*c*		
La	5.4267(3)	28.013(2)	5.4805(3)	833.13(9)	0.063
Pr	5.3908(3)	27.603(2)	5.4737(3)	814.52(9)	0.070

in the RP nickelate lattice. Whatever the segregation mechanism, the corresponding error in the measured δ values of $Pr_4Ni_{2.7}Fe_{0.3}O_{10\pm\delta}$ was estimated to be lower than 0.004, comparable to experimental uncertainty of TGA and CT techniques. The SAED patterns were all indexed taking into account the extinction rules for *Cmca* symmetry. As an example, Fig. 5 shows two SAED patterns where the reflections correspond to atomic layers sequence along the *b*-axis. Notice that, while neither diffuse scattering nor intergrowth phenomena were detected in these preliminary electron microscopy studies, detailed structural investigations are now in progress. The unit cell parameters and volume of as-synthesized $Ln_4Ni_{2.7}Fe_{0.3}O_{10}$ (Table 2) are larger than those of parent $Ln_4Ni_3O_{10}$ [11,21], in accordance with the cation radii of high-spin Fe^{3+} and Ni^{3+} [22]. For comparison, the lattice parameters of undoped lanthanum nickelate were reported as $a = 5.415(1)$ Å, $b = 5.465(1)$ Å, $c = 27.959(9)$ Å for $La_4Ni_3O_{10.0}$ (space group *Fmmm* [11]), and $a = 5.41327(11)$ Å, $b = 5.46233(11)$ Å, $c = 27.9605(7)$ Å for $La_4Ni_3O_{10.03}$ (space group *Bmab* [21]). Notice that the *c* parameter calculated for *Fmmm* and *Bmab* space groups corresponds to *b* for the *Cmca* symmetry. In case of $Pr_4Ni_3O_{9.85}$ (space group *Fmmm*), the lattice constants were $a = 5.370(1)$ Å, $b = 5.462(1)$ Å and $c = 27.528(7)$ Å [11]. Analogously, the unit cell parameters and volume of $Pr_4Ni_{2.7}Fe_{0.3}O_{10}$ are substantially smaller compared to $La_4Ni_{2.7}Fe_{0.3}O_{10}$ (Table 2) due to the smaller size of praseodymium cations with respect to La^{3+} [22]. In comparison with the parent nickelates [11], the difference in lattice parameters of $Ln_4Ni_{2.7}Fe_{0.3}O_{10}$ phases containing different rare-earth cations is considerably higher. The latter tendency might suggest that for $Pr_4Ni_{2.7}Fe_{0.3}O_{10}$, the average oxidation state of nickel is higher than in $La_4Ni_{2.7}Fe_{0.3}O_{10}$ and/or a small fraction of Pr^{4+} may be present in the lattice. This assumption fits well to the oxygen stoichiometry data discussed below.

The room temperature Mössbauer spectrum of $La_4Ni_{2.7}Fe_{0.3}O_{10}$ consists of two absorption peaks with different areas (Fig. 6A). This spectrum may only be analyzed considering, at least, two quadrupole doublets. Consequently, the $La_4Ni_{2.7}Fe_{0.3}O_{10-\delta}$ spectrum collected at 4 K (Fig. 6B), when the magnetic hyperfine interactions are observed, may only be described with at least two magnetic sextets. The parameters estimated from the Mössbauer spectra are summarized in Table 1. The isomer shifts are typical for Fe^{3+} ions in oxide compounds; no traces of Fe^{4+} or Fe^{2+} can be detected. The presence of two contributions with relative areas ratio close to 2:1 indicates an essentially random distribution of Fe^{3+} between the two non-equivalent crystallographic sites occupied by the transition metal cations in $La_4Ni_{2.7}Fe_{0.3}O_{10}$ lattice, Ni1 and Ni2 (Fig. 1). The Ni2 site, where Fe^{3+} concentration is approximately twice higher, has also larger quadrupole splitting (QS, Table 1). The latter phenomenon results from the fact that the nickel–oxygen polyhedra involving Ni2 positions are significantly distorted, whereas distortion of the coordination octahedra near Ni1 sites is almost negligible [21,23]. In the case of $Pr_4Ni_{2.7}Fe_{0.3}O_{10}$, the resolution of room-temperature Mössbauer spectrum (Fig. 6C) is insufficient to evaluate Fe^{3+} distribution between the nickel sites, but the estimated average parameters are similar to $La_4Ni_{2.7}Fe_{0.3}O_{10}$.

TGA showed that $Ln_4Ni_{2.7}Fe_{0.3}O_{10\pm\delta}$ exhibit a minor oxygen hyperstoichiometry at low temperatures and become oxygen-deficient on heating (Table 2 and Fig. 7). The deviations from stoichiometric oxygen content in $Ln_4Ni_{2.7}Fe_{0.3}O_{10-\delta}$ at atmospheric oxygen partial pressure remain relatively low (Fig. 7A). Furthermore, the temperature dependencies of equilibrium oxygen deficiency in the

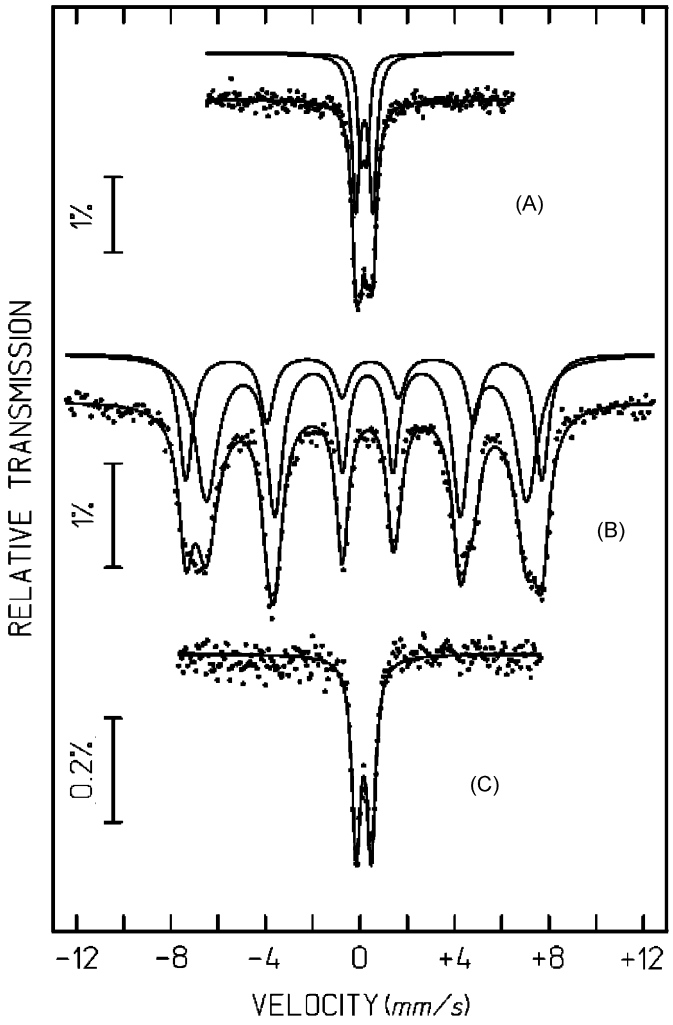

Fig. 6. Mössbauer spectra of $La_4Ni_{2.7}Fe_{0.3}O_{10+\delta}$ at 295 K (A) and 4 K (B), and of $Pr_4Ni_{2.7}Fe_{0.3}O_{10+\delta}$ at 295 K (C). The curves plotted on the experimental points are a quadrupole doublet (C), the sum of two magnetic sextets (B) and the sum of two quadrupole doublets (A), the latter shown slightly shifted for clarity.

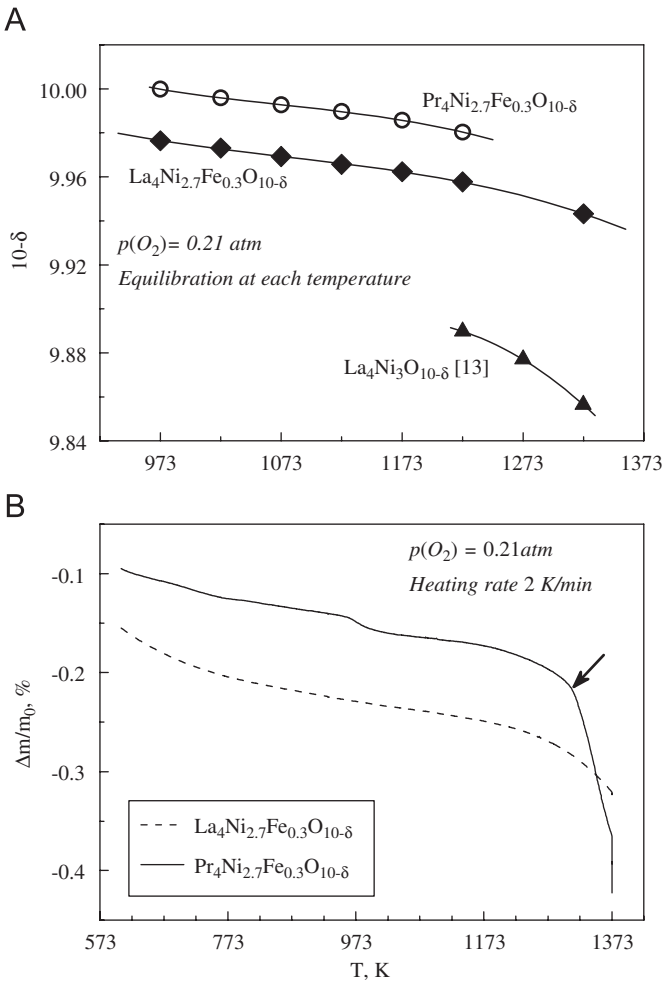

Fig. 7. Temperature dependencies of the equilibrium oxygen non-stoichiometry of $La_4Ni_{2.7}Fe_{0.3}O_{10-\delta}$ and $Pr_4Ni_{2.7}Fe_{0.3}O_{10-\delta}$ at atmospheric oxygen partial pressure in comparison with literature data [13] on parent $La_4Ni_3O_{10-\delta}$ (A), and relative weight changes measured in the continuous heating regime in air (B). The arrow in (B) shows approximate phase stability boundary.

La- and Pr-containing compositions are very similar; the changes in δ values at 973–1223 K in air are 0.019 and 0.020, respectively. The total oxygen content is, however, higher for $Pr_4Ni_{2.7}Fe_{0.3}O_{10-\delta}$, confirming the presence of a small amount of Pr^{4+} or moderately higher oxidation state of nickel cations. The latter seems more likely and may appear due to compensation of the lattice stress induced by decreasing rare-earth cation radius. Another necessary comment is that the difference in the δ values of $La_4Ni_{2.7}Fe_{0.3}O_{10-\delta}$ and $Pr_4Ni_{2.7}Fe_{0.3}O_{10-\delta}$, 0.023–0.024 at 973–1223 K and atmospheric $p(O_2)$, is significantly higher than the experimental error estimated as 0.002.

When compared to undoped $La_4Ni_3O_{10-\delta}$ [13], the oxygen content in $La_4Ni_{2.7}Fe_{0.3}O_{10-\delta}$ is much closer to the stoichiometric value (Fig. 7A). This originates from the higher oxidation state of iron cations, predominantly trivalent, with respect to $Ni^{3+/2+}$. The presence of statistically distributed $Fe^{3+}O_6$ octahedra is expected to increase average coordination of nickel ions and, thus, to stabilize the RP lattice; analogous phenomena are well known for oxygen-deficient perovskites [15]. Indeed, as shown below, the decomposition of $La_4Ni_{2.7}Fe_{0.3}O_{10-\delta}$ into $La_2Ni(Fe)O_{4+\delta}$ and NiO occurs at lower oxygen pressures if compared to $La_4Ni_3O_{10-\delta}$. The average Ni oxidation state in $La_4Ni_{2.7}Fe_{0.3}O_{10-\delta}$, 2.59–2.61 at 973–1323 K in air, is also slightly higher than that in the parent nickelate [13].

In spite of the high oxygen content, an opposite situation is however observed for $Pr_4Ni_{2.7}Fe_{0.3}O_{10-\delta}$ due to the smaller radius of praseodymium cations, which is another key factor determining thermodynamic stability of the RP phases. Heating of $Pr_4Ni_{2.7}Fe_{0.3}O_{10-\delta}$ above 1310–1330 K in air leads to drastic weight changes caused by the phase transition into $Pr_2Ni(Fe)O_{4+\delta}$ solid solution with K_2NiF_4-type structure (Figs. 7B and 8). The decomposition temperature of $Pr_4Ni_{2.7}Fe_{0.3}O_{10-\delta}$ is, again, in a good agreement with literature data on Pr_2NiO_4-based phases [16,24], and is significantly lower than those of

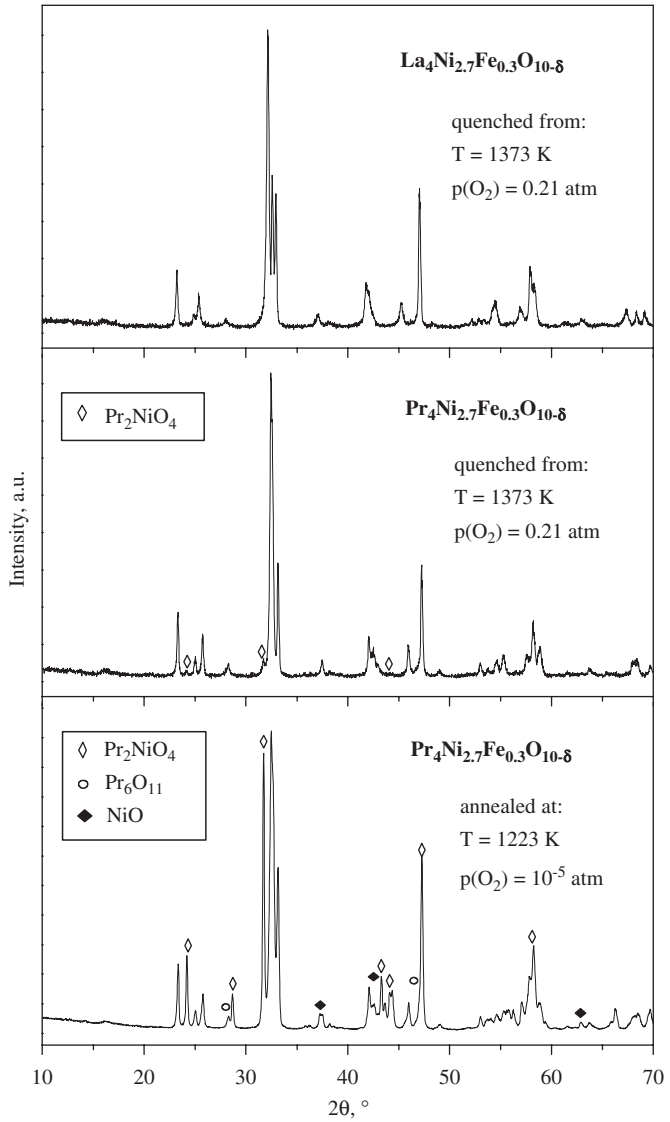

Fig. 8. XRD patterns of $Ln_4Ni_{2.7}Fe_{0.3}O_{10-\delta}$ samples, quenched after annealing at 1373 K in air and at 1223 K in flowing argon for 75 h. The symbols show major peaks of the secondary phases formed on decomposition of $Pr_4Ni_{2.7}Fe_{0.3}O_{10-\delta}$, namely the Pr_2NiO_4-based solid solution and binary nickel and praseodymium oxides. No decomposition was observed for $La_4Ni_{2.7}Fe_{0.3}O_{10-\delta}$ annealed at 1373 K in air.

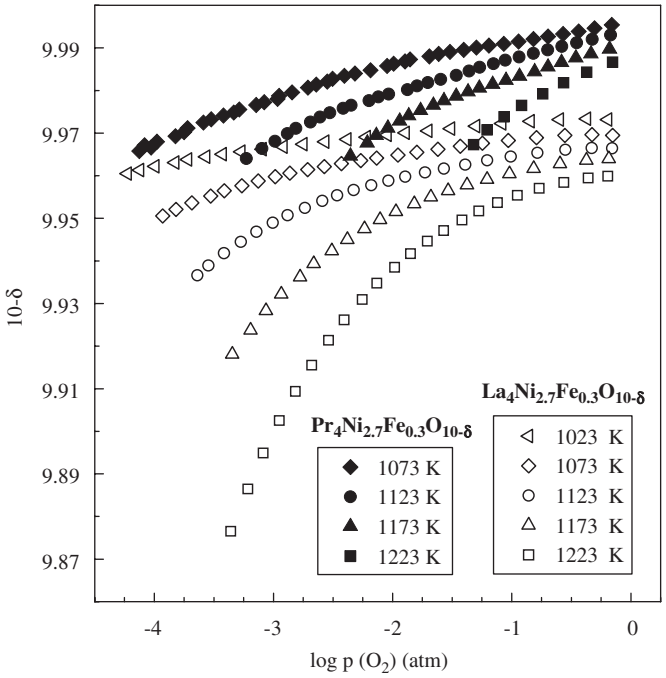

Fig. 9. The $p(O_2)$-T-δ diagrams of $La_4Ni_{2.7}Fe_{0.3}O_{10-\delta}$ and $Pr_4Ni_{2.7}Fe_{0.3}O_{10-\delta}$ at 1023–1223 K.

$La_4Ni_{2.7}Fe_{0.3}O_{10-\delta}$ and even $La_4Ni_3O_{10-\delta}$. Note that the stability of most perovskite-related compounds, including the RP nickelates and cuprates, becomes lower when the A-site cation radius and tolerance factor decrease (see, for instance, [11,15,25] and references therein). Most likely, the same mechanism is responsible for the surface segregation of praseodymium oxide in as-prepared $Pr_4Ni_{2.7}Fe_{0.3}O_{10-\delta}$; possible formation of Pr^{4+} cations should also have a strong lattice-destabilizing effect. The dissolution of praseodymium oxide in $Pr_4Ni_{2.7}Fe_{0.3}O_{10-\delta}$ lattice occurs on heating up to 940–970 K and is accompanied with weight losses visible in the TGA curves (Fig. 7B).

Fig. 9 presents the $p(O_2)$-T-δ diagrams of $Ln_4Ni_{2.7}Fe_{0.3}O_{10-\delta}$ under oxidizing conditions, within the domains where the orthorhombic RP phases exist. Both title materials display qualitatively similar trends, which are, however, far from those predicted by the ideal-solution model [26]. The observed behavior is also different from that of the K_2NiF_4-type nickelates, where the δ vs. $\log p(O_2)$ dependencies are almost linear [9,14]. In the case of $Ln_4Ni_{2.7}Fe_{0.3}O_{10-\delta}$, these dependencies show a substantial non-linearity; their slope increases remarkably on increasing temperature and on reducing $p(O_2)$, probably due to close proximity of the phase boundary. Reduction leads to phase decomposition accompanied with stepwise changes in the oxygen content (Figs. 3, 7B and 10). The decomposition processes were found reversible, except for standard hysteresis phenomena (Fig. 10). XRD analysis of reduced $Ln_4Ni_{2.7}Fe_{0.3}O_{10-\delta}$ showed that in all cases, Ln_2NiO_4-based solid solutions are formed, although the decomposition of $Pr_4Ni_{2.7}Fe_{0.3}O_{10-\delta}$ involves praseodymium oxide separation (Fig. 8) and has hence a more complex mechanism than suggested for lanthanum nickelate [13]. One should also mention that, if compared to the La-containing composition, $Pr_4Ni_{2.7}Fe_{0.3}O_{10-\delta}$ exhibits a considerably narrower range of the oxygen non-stoichiometry variations where the RP phase exists. This type of behavior can be easily predicted considering the lower thermodynamic stability of $Pr_4Ni_{2.7}Fe_{0.3}O_{10-\delta}$ (Fig. 7B).

Fig. 11 compares the low-$p(O_2)$ phase boundaries of $La_4Ni_{2.7}Fe_{0.3}O_{10-\delta}$ and $Pr_4Ni_{2.7}Fe_{0.3}O_{10-\delta}$, estimated from the CT and TGA results as illustrated in Figs. 3 and 7B. These results are compared to the data on $La_4Ni_3O_{10-\delta}$ [12], $La_2NiO_{4+\delta}$ [12], $La_2Ni_{0.9}Fe_{0.1}O_{4+\delta}$ [14], $Pr_2NiO_{4+\delta}$ [16], $Pr_2Ni_{0.9}Fe_{0.1}O_{4+\delta}$ [16] and NiO [27]. The equilibrium oxygen pressure corresponding to the $Pr_2NiO_4 \leftrightarrow Pr_4Ni_3O_{10} + PrO_x$ transition, is also shown. The latter value

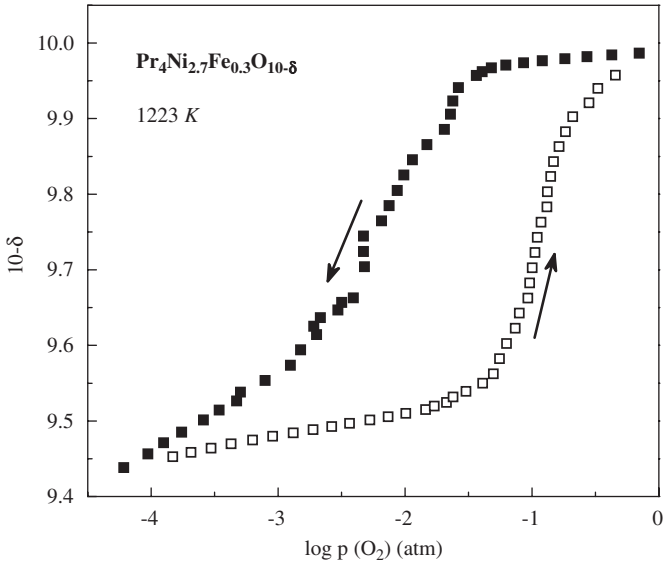

Fig. 10. Typical hysteresis of oxygen content variations on re-oxidation of $Pr_4Ni_{2.7}Fe_{0.3}O_{10-\delta}$ at 1223 K. Arrows indicate the direction of $p(O_2)$ changes.

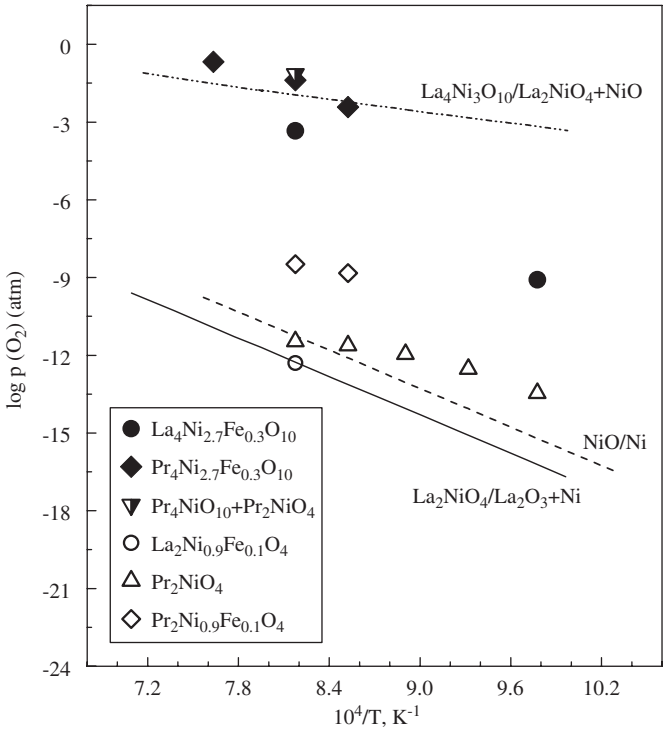

Fig. 11. Comparison of the low-$p(O_2)$ stability limits of $La_4Ni_{2.7}Fe_{0.3}O_{10-\delta}$, $Pr_4Ni_{2.7}Fe_{0.3}O_{10-\delta}$ and $Pr_4Ni_3O_{10-\delta}$ phases, determined by the coulometric titration and thermogravimetry (see text). Data on other Ni-containing oxide compounds [12,14,16,27] are shown for comparison.

was obtained by CT of the decomposition products of $Pr_2NiO_{4+\delta}$, which transforms into the mixture of $Pr_4Ni_3O_{10-\delta}$ and praseodymium oxide on oxidation below 1200 K [16,24]; the transition at 1223 K is completely reversible (Fig. 12), making it possible to precisely determine phase boundary. The obtained $p(O_2)$ value is

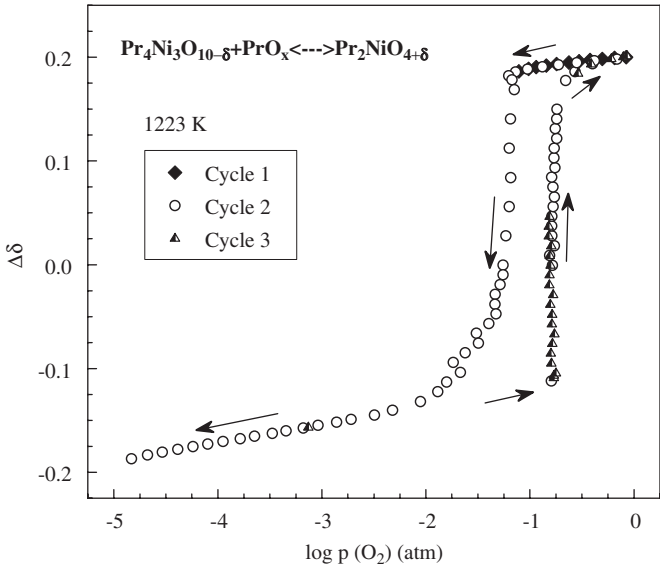

Fig. 12. Oxygen content variations in a multiphase oxide mixture with the Pr:Ni cation ratio of 2.0, where the $Pr_2NiO_{4+\delta}$, $Pr_4Ni_3O_{10-\delta}$ and PrO_x phases are formed on cycling of oxygen partial pressure.

in excellent agreement with the stability limit of $Pr_4Ni_{2.7}Fe_{0.3}O_{10-\delta}$ (Fig. 11). These results confirm that the thermodynamic stability of $Pr_4Ni_3O_{10-\delta}$ is lower than that of $La_4Ni_3O_{10-\delta}$, and is essentially unaffected by iron doping. On the contrary, the incorporation of Fe^{3+} cations in $La_4Ni_3O_{10-\delta}$ clearly shifts the decomposition boundary towards lower oxygen pressures, although the apparent stability limit at 1023 K may be lower than the true value due to a slow phase-transformation kinetics limited by cation diffusion. It should also be mentioned that the partial substitution of iron for nickel has no influence on the low-$p(O_2)$ stability boundary of $La_2NiO_{4+\delta}$, but decreases stability of $Pr_2NiO_{4+\delta}$.

Finally, Fig. 13 shows the partial molar enthalpy (Δh_0) for oxygen incorporation into the lattices of $La_4Ni_{2.7}Fe_{0.3}O_{10-\delta}$ and $Pr_4Ni_{2.7}Fe_{0.3}O_{10-\delta}$. This quantity, related to one mole of oxygen atoms, was calculated from the temperature dependencies of equilibrium oxygen partial pressure at fixed oxygen non-stoichiometry:

$$\Delta h_0 = \frac{R}{2}\left[\frac{\partial \ln p(O_2)}{\partial(1/T)}\right]_{\delta}. \quad (1)$$

For $Ln_4Ni_{2.7}Fe_{0.3}O_{10-\delta}$, these estimations are rather rough due the narrow phase existence domains and non-ideal behavior of the oxygen sublattices; the partial molar enthalpy is thus given for the limited temperature ranges where the curvature of $\ln p(O_2)$ vs. $1/T$ dependencies can be neglected. Nevertheless, the estimated Δh_0 values are consistent with the oxygen-incorporation enthalpy in K_2NiF_4-type $La_2Ni_{0.9}Fe_{0.1}O_{4+\delta}$ [14]. When total oxygen content in the nickelate-based lattices increases, further intercalation becomes less energetically favorable due to increasing coulombic repulsion between O^{2-} anions. Similar mechanism is relevant to the relationship between Δh_0 values of oxygen-deficient $Ln_4Ni_{2.7}Fe_{0.3}O_{10-\delta}$ and

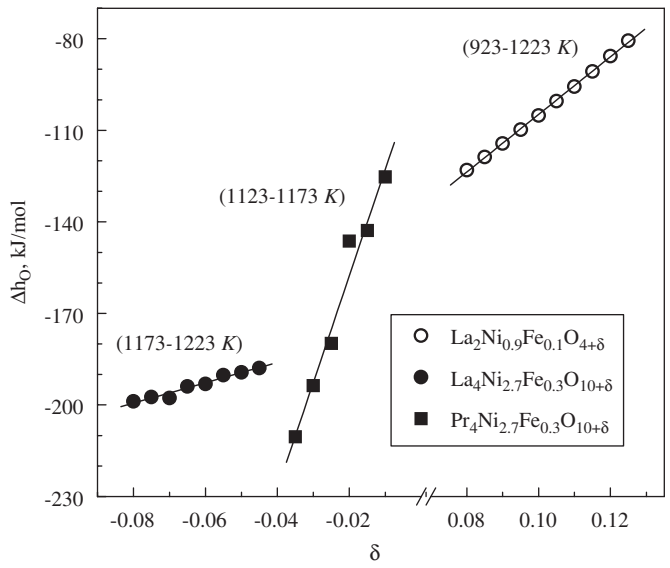

Fig. 13. Partial molar enthalpy for oxygen incorporation into the lattice of $La_4Ni_{2.7}Fe_{0.3}O_{10-\delta}$ and $Pr_4Ni_{2.7}Fe_{0.3}O_{10-\delta}$, calculated using Eq. (1), as function of the oxygen non-stoichiometry. Solid lines are for visual guidance only.

oxygen-hyperstoichiometric $La_2Ni_{0.9}Fe_{0.1}O_{4+\delta}$. The oxygen thermodynamics of the latter compound is heavily affected by strong anion–anion repulsion [9], which impedes incorporation of extra oxygen and is reflected by the relatively low absolute values of the partial molar enthalpy. In the case of $Pr_4Ni_{2.7}Fe_{0.3}O_{10-\delta}$, abnormally large variations of Δh_0 are associated with the close proximity of the phase transition induced by a small increment in the oxygen content.

4. Conclusions

The iron-substituted layered nickelates $Ln_4Ni_{2.7}Fe_{0.3}O_{10-\delta}$ (Ln = La, Pr) with orthorhombic Ruddlesden-Popper type structure (space group *Cmca*) were synthesized via glycine-nitrate process and studied by the CT and thermogravimetric analysis at 973–1223 K. In air, both compounds exhibit minor oxygen excess at low temperatures and become oxygen-deficient on heating above 700–950 K. Increasing temperature above 1300 K leads to phase decomposition. The oxygen deficiency at 973–1223 K and atmospheric oxygen partial pressure varies in the narrow ranges $(2.4–4.2)\times10^{-2}$ and $(0.01–2.0)\times10^{-2}$ atoms per formula unit for the La- and Pr-containing compositions, respectively. Doping of $La_4Ni_3O_{10-\delta}$ with iron decreases oxygen non-stoichiometry, shifting the low-$p(O_2)$ stability boundary towards more reducing conditions due to stabilization of the transition metal–oxygen octahedra. The Mössbauer spectroscopy studies confirmed that iron cations are predominantly trivalent and are distributed statistically between the non-equivalent nickel sites. In the case of $Pr_4Ni_{2.7}Fe_{0.3}O_{10-\delta}$, decreasing A-site cation radius leads to considerably lower stability compared to $La_4Ni_{2.7}Fe_{0.3}O_{10-\delta}$ and $La_4Ni_3O_{10-\delta}$, although the oxygen content in $Pr_4Ni_{2.7}Fe_{0.3}O_{10-\delta}$ is closer to the stoichiometric value. The partial substitution of iron for nickel has no essential effect on the low-$p(O_2)$ decomposition limit of $Pr_4Ni_3O_{10-\delta}$, indicating that the thermodynamic stability is primarily determined by crystallographic factors, namely the cation size matching in RP nickelate structure. The partial molar enthalpies for oxygen incorporation into $Ln_4Ni_{2.7}Fe_{0.3}O_{10-\delta}$ lattices lie in the range from −210 to −125 kJ/mol at 1123–1223 K, decreasing when oxygen deficiency increases. The results show that, for the use of $Ln_4(Ni,Fe)_3O_{10}$-based phases as cathode materials of intermediate-temperature SOFCs, the sintering temperature of porous electrode layers should be limited to 1250–1300 K. The oxygen activity variations under cathodic conditions should be tolerated by $Ln_4Ni_{2.7}Fe_{0.3}O_{10-\delta}$ lattices if the SOFC operation temperature is lower than 1100 K.

Acknowledgments

This work was partially supported by the FCT, Portugal (projects POCI/CTM/59197/2004, SFRH/BPD/17649/2004, SFRH/BPD/28629/2006 and REEQ/710/CTM/2005), and the MatSILC project (STRP 033410, CEC).

References

[1] B. Vigeland, R. Glenne, T. Breivik, S. Julsrud, Int. Patent Application PCT WO 99/59702, 1999.
[2] G. Amow, I.J. Davidson, S.J. Skinner, Solid State Ionics 177 (2006) 1205.
[3] M. Al Daroukh, V.V. Vashook, H. Ullmann, F. Tietz, I.A. Raj, Solid State Ionics 158 (2003) 141.
[4] E. Boehm, J.-M. Bassat, M.C. Steil, P. Dordor, F. Mauvy, J.-C. Grenier, Solid State Sci. 5 (2003) 973.
[5] F. Mauvy, C. Lalanne, J.M. Bassat, J.C. Grenier, H. Zhao, Ph. Dordor, P. Stevens, J. Eur. Ceram. Soc. 25 (2005) 2669.
[6] V.V. Kharton, A.P. Viskup, A.V. Kovalevsky, E.N. Naumovich, F.M.B. Marques, Solid State Ionics 143 (2001) 337.
[7] V.V. Kharton, A.A. Yaremchenko, A.L. Shaula, M.V. Patrakeev, E.N. Naumovich, D.I. Logvinovich, J.R. Frade, F.M.B. Marques, J. Solid State Chem. 177 (2004) 26.
[8] V.V. Kharton, E.V. Tsipis, A.A. Yaremchenko, J.R. Frade, Solid State Ionics 166 (2004) 327.
[9] E.N. Naumovich, M.V. Patrakeev, V.V. Kharton, A.A. Yaremchenko, D.I. Logvinovich, F.M.B. Marques, Solid State Sci. 7 (2005) 1353.
[10] J. Jorgensen, B. Dabrowski, S. Pei, D. Richards, D. Hinks, Phys. Rev. B 40 (1989) 2187.
[11] Z. Zhang, M. Greenblatt, J. Solid State Chem. 117 (1995) 236.
[12] M. Zinkevich, F. Aldinger, J. Alloys Compd. 375 (2004) 147.
[13] D.O. Bannikov, V.A. Cherepanov, J. Solid State Chem. 179 (2006) 2721.
[14] E.V. Tsipis, E.N. Naumovich, M.V. Patrakeev, J.C. Waerenborgh, Ye.V. Pivak, P. Gaczyński, V.V. Kharton, J. Phys. Chem. Solids (2007), in press, doi:10.1016/j.pcs.2007.04.006.
[15] V.V. Kharton, A.A. Yaremchenko, E.N. Naumovich, J. Solid State Electrochem. 3 (1999) 303.
[16] A.V. Kovalevsky, V.V. Kharton, A.A. Yaremchenko, Y.V. Pivak, E.V. Tsipis, S.O. Yakovlev, A.A. Markov, E.N. Naumovich, J.R. Frade, J. Electroceram. (2007), in press, doi:10.1007/S10832-007-9024-7.

[17] L.A. Chick, L.R. Pederson, G.D. Maupin, J.L. Bates, L.E. Thomas, G.J. Exarhos, Mater. Lett. 10 (1990) 6.
[18] M.V. Patrakeev, E.B. Mitberg, A.A. Lakhtin, I.A. Leonidov, Ionics 4 (1998) 191.
[19] G.J. Long, T.E. Cranshaw, G. Longworth, Mossb. Effect. Ref. Data J. 6 (1983) 42.
[20] J.C. Waerenborgh, M.O. Figueiredo, J.M.P. Cabral, L.C.J. Pereira, J. Solid State Chem. 111 (1994) 300.
[21] C.D. Ling, D.N. Argyriou, G.-Q. Wu, J.J. Neumeier, J. Solid State Chem. 152 (2000) 517.
[22] R.D. Shannon, Acta Cryst. A 32 (1976) 751.
[23] V.I. Voronin, I.F. Berger, V.A. Cherepanov, L.Ya. Gavrilova, A.N. Petrov, A.I. Ancharov, B.P. Tolochko, S.G. Nikitenko, Nucl. Instrum. Methods Phys. Res. Sect. A 470 (2001) 202.
[24] P. Odier, Ch. Allançon, J.M. Bassat, J. Solid State Chem. 153 (2000) 381.
[25] M. Greenblatt, Curr. Opin. Solid State Mater. Sci. 2 (1997) 174.
[26] P. Kofstad, Nonstoichiometry, Diffusion and Electrical Conductivity in Binary Metal Oxides, Wiley-Interscience, New York, 1972.
[27] H. Yokokawa, N. Sakai, T. Kawada, M. Dokiya, Denki Kagaku 58 (1990) 489.